THE DAY AFTER: POST-COLLISION DISTRIBUTION OF REMNANTS, FRAGMENTS AND DEBRIS CLOUDS IN THE OUTER SOLAR SYSTEM

G. Sarid and J. Larson
University of Central Florida, Florida Space Institute and Department of Physics, 12354 Research Parkway, Orlando, FL 32826, U.S.A (gal.sarid@ucf.edu).

Introduction: Collisions that deform and disrupt both target and projectile bodies change the configuration of the original system. It produces remnant bodies that may differ in composition, angular momentum and orbit. These can span a large size range, from the target body itself, to smaller satellites, to ejected fragments, even down to unbound clouds of fine debris [1, 2].

Erosive collisions have been invoked to explain several outstanding issues in the inner solar system, such as Moon formation [3, 4], Mercury's origin [5, 6], iron meteorite parent bodies [7, 8].

In the outer solar system, there is increasing evidence that multiple systems exist in complex physical states, which probably formed and evolved early, largely through erosive/disruptive collisions between at least partially differentiated bodies. These include Pluto's compact moon system [9], Haumea's collisional family [10], several binary or single satellite systems (e.g, 1999 TC36, Eris, Quaoar and several Centaur objects) [11] and even ring systems around Centaurs, which may have embedded tiny moons [12, 13]. Despite multiple dynamical perturbations and potential close-encounters with planets, it seems that bound systems can survive transport, migration and scatter interactions to be detectable today.

We are interested in understanding the fate of the released material as an orbital distribution. This can be either bound material, as disks or satellites, or unbound fragments, debris clouds. The residual material that is not accreted within the first 1-2 days after a collision event and has velocities greater than the mutual escape velocity of the target-bound system, may experience short and long-term dynamical perturbations and evolve on diverging orbits.

Methodology: The internal thermal and chemical configuration of our presumed colliding bodies are taken from a large suite of previously calculated evolution models for icy bodies and assumed chondritic composition for rocky bodies [14, 15, 16]. We have conducted 3D numerical simulations of collisions between icy-rocky bodies utilizing *GADGET2*, which is an SPH code modified to handle tabulated equations of state [17]. These simulations have covered a range in projectile and target/projectile mass ratios, impact velocities (~1-7times the mutual escape velocity) and impact angles, corresponding to events of head-on collisions to barely grazing encounters [14, 15, 16].

We follow the long-term evolution of unbound collision remnants and debris by employing an N-body calculation scheme (*Mercury* for robust low-resolution cases, *REBOUND* for high-resolution and non-symplectic cases) [18, 19]. We include all planets and additional gravitational potentials from the nearby surviving target (and projectile) body. Through this calculation we will statistically determine plausible trajectories and re-accumulation paths of ejected material.

The short-term gravitational evolution of material released through a collision is tracked self-consistently within *GADGET2*. For post-collision systems that seem to retain large clumps of material in bound configurations about the main (target) body, we cast the bound moons as massless particles in the *Mercury* simulation and calculate the long-term stability of the system.

Results: One main observable that can be influenced by collision history is the bulk density [20, 21]. Fig. 1 shows how the ratio of satellite mass to total mass (designated as q) relates to the primary body's density. In black are TNO systems with well-measured components and associated uncertainties [21]. Blue symbols represent our analysis of a set of collision simulations between fully-differentiated bodies (core, mantle and icy crust). This suite was run with initial object radii of 150-1200 km, impact velocities of 0.5-5 km/s and impact angles of 0-60 degrees. Each simulation included 25K-100K particles and full EOS for water ice, serpentine and silica.

For our analysis interpretation we assumed zero-porosity densities, grazing collisions included only if a remnant other than the target and impactor bodies exists (some erosion) and minimal size of body is 100 SPH particles (avoid spurious smoothing length, corresponding to ~40-100 km).

Fig. 2 shows an example calculation for the orbital diffusion of collision ejecta around the primary's orbit. The example here is for Centaur 10199 Chariklo (semi-major axis at 15.8 AU and 150 km radius). The fragments are approximated as 500 massless particles, initialized at random within an orbital element cube of size $da/a = de/e/di/i = 10^{-5}$ (semi-major axis, a, eccentricity, e, and inclination, i). The other orbital angles were chosen randomly. This setup has fragments initially at up to 23,600 km from Chariklo and with very small deviations from its Keplerian velocity (~7.5

km/s). This choice of initial conditions is comparable with wide-binary configurations in the outer solar system [11, 22]. This means that the particles are near a minimally-bound initial orbit relative to the primary.

The orbits of the the fragments evolve due to the cumulative gravitational perturbations, but predominantly due to near-resonant interactions with Uranus. The separation (in AU) and dispersion (in km/s) evolve through time, relative to Chariklo's orbit, to cover a large range of $3x10^5$ km to 70 AU and 10^{-4} to 5 km/s, respectively. This is represented in gray, for up to 1M yrs of simulated time. We note that the mean values, color-coded from 1Kyr to 1M yr, start diverging more rapidly after the first ~10 Kyr. After ~50 Kyr the mean velocity dispersion is > 200 m/s, and the mean separation is > 0.5 AU. From an identification standpoint, it means that a dynamical association becomes very hard to distinguish. Thus, a multi-component system would be much less probable to be associated with Chariklo, beyond 50 Kyr from the ejection event.

If we compare our interpretation with Chariklo's recently-discovered ring system, which is much more tightly bound [12], we can say that the observed system has to be young. This should hold if the the formation mechanism is collisional ejection and/or satellite disruption, despite a postulated ring configuration being seemingly stable to dynamical interactions [23].

Acknowledgements: GS thanks FSI for continued support, through SRI awards and discretionary funds.

References: [1] Asphaug, E. (2010) *Chemie der Erde*, 70, 199. [2] Asphaug, E., Collins, G. & Jutzi, M. (2015) *Asteroids IV*, U. of Arizona Press, 661. [3] Cuk, M. and Stewart, S. T. (2012) *Nature, 338*, 1047. [4] Canup, R. M. 2012, *Science*, 338, 1052. [5] Benz, W. et al. (2007) *SSRev*., 132, 189. [6] Sarid, G., Stewart, S. T., & Leinhardt, Z. M. (2014) *LPI Cont.*, 45, 2723. [7] Burbine, T. H. et al. (2002), *Asteroids III*, U. of Arizona Press, 653. [8] Goldstein, J. I. et al. (2009), *Chemie der Erde*, 69, 293. [9] Canup, R. (2011) *AJ, 141*, 35. [10] Brown M. E. et al. (2007) *Nature, 446*, 294-296. [11] Noll. K. et al .(2008) *The Solar System Beyond Neptune*, U. Arizona Press, 345-363. [12] Braga-Ribas, F. et al. (2014) *Nature*, 508, 72. [13] Ortiz, J. L. et al. (2015) *A&A*, 576, A18. [14] Sarid, G. & Stewart S. T. (2013) *LPI Cont.*, 44, 1467. [15] Sarid, G. & Stewart S. T. (2015) *LPI Cont.*, 46, 2834. [16] Sarid, G., Stewart, S. T., & Leinhardt, Z. M. (2016) IAU Proceedings, 318, 9. [17] Marcus, R. A. (2009) *AJ, 700*, L118-L122. [18] Chambers, J. E. (1999) *MNRAS*, 304, 793. [19] Rein H. & Liu S.-F. (2012) *A&A*, 537, A128. [20] Brown, M. E. (2012), *AREPS*, 40, 467. [21] Barr, A. C. & Schwamb, M. E. (2016), MNRAS, 460, 1542. [22] Sheppard, S. S., Ragozzine, D. & Trujillo, C. (2012), *AJ*, 143, 58. [23] Araujo, R. , Sfair, A. N., R. & Winter, O. C. (2016), ApJ, 824, 80.

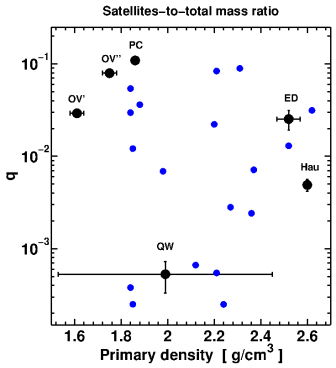

Figure 1: Satellite-to-total mass ratio, q, as a function of the primary body density. **Black** symbols are measured values and errors for Orcus-Vanth (OV, 2 values due to albedo uncertainties), Pluto-Charon (PC), Quaoar-Weywot (QW), Eris-Dysnomia (ED) & the Haumea family (Hau), reproduced from [21]. **Blue** symbols are results from our calculations of energetic collisions between differentiated dwarf planets with a range of collision parameters.

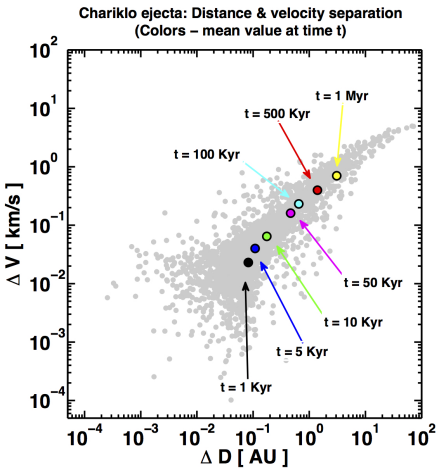

Figure 2: Distribution of fragments around 10199 Chariklo's orbit, following gravitational perturbations with current solar system orbital conditions. Separation (relative distance, D, in AU) & dispersion (relative velocity, V, in km/s) are calculated for snapshots between 1Kyr-1Myr. In gray is the distribution of all particles throughout the simulation. In color are the mean values for the fragment population at each recorded time (designated with a color arrow). See text for further analysis.